Materials Today Physics 14 (2020) 100228

Contents lists available at ScienceDirect

Materials Today Physics

journal homepage: https://www.journals.elsevier.com/materials-today-physics

Strong band filling induced significant excited state absorption in $MAPbI_3$ under high pump power

B.A. Chen [a, c], G.T. Pang [a, c], X.Q. Lan [b], Z.B. He [b], R. Chen [a, *]

[a] Department of Electrical and Electronic Engineering, Southern University of Science and Technology, Shenzhen, 518055, China
[b] Department of Materials Science and Engineering, Shenzhen Key Laboratory of Full Spectral Solar Electricity Generation (FSSEG), Southern University of Science and Technology, Shenzhen, 518055, China

ARTICLE INFO

Article history:
Received 10 April 2020
Received in revised form
1 May 2020
Accepted 2 May 2020
Available online 15 May 2020

Keywords:
Perovskite
Carrier dynamics
Transient absorption
Hot phonon bottleneck
Auger effect

ABSTRACT

Perovskite has been considered as promising material for solar cell application. Understanding the carrier dynamics in perovskite material plays a vital role for further improvement of the power conversion efficiency of solar cells. In this article, carrier dynamics of $MAPbI_3$ under different pump powers have been investigated by ultrafast pump-probe transient absorption spectroscopy. Complete processes of carrier cooling and recombination under different pump powers have been characterized and compared carefully. It is found that a significant carrier band filling happened during cooling process under high pump power, which results in a strong excited state absorption at the photon energy of 2.353 eV. High carrier density induced strong Auger effect appears not only in the band edge but also the higher conduction band. And subsequently, a large part of carriers keeps hot for more than 5 ns indicating that $MAPbI_3$ is meaningful for hot carrier extraction in solar cells. A critical carrier concentration of 9.32×10^{17} cm^{-3} has been determined at which Auger effect starts to work. It could provide some guidance for perovskite solar cell application.

1. Introduction

Lead iodide perovskite material has been regarded as the promising candidate for solar cell because of its extraordinary physical properties such as long carrier lifetime [1,2], large diffusion coefficient [3,4], and strong light absorption. At present, the perovskite solar cell possesses a power conversion efficiency (PCE) above 23% which is close to that (26.6%) of silicon-based solar cells [5–8]. Hot carrier-based perovskite solar cell is expected to break the Shockley-Queisser limit existed in conventional single junction photovoltaic device by extracting hot carriers from perovskite light absorber before they cool to band edge [9–13]. Intrinsic photophysical properties of carrier dynamics, such as carrier thermalization, carrier cooling, band filling, and bandgap renormalization, have been intensively investigated to improve the overall PCE of the solar cell [14–17]. Pump power shows a significant influence on the carrier dynamics, which is usually characterized by ultrafast pump-probe transient absorption spectra and exhibits different cooling and recombination mechanisms [18–22]. Previous researches mainly focus on the carrier dynamics at the bandgap and usually performed under moderate pump power to avoid sample damage. However, lots of hot carriers will be generated under higher pump power and subsequently result in a hot phonon bottleneck, which will slow down the carrier cooling rate inside the perovskite material [23,24]. Unfortunately, investigation of the carrier dynamics in perovskite material under high pump power is still scarce.

In this article, the carrier dynamics of $MAPbI_3$ under high pump power have been investigated. Complete processes of carrier thermalization, carrier cooling, and carrier recombination under different pump powers have been characterized and compared. Ultrafast transient absorption spectra of $MAPbI_3$ show significant differences under low and high power excitation. There is a strong excited state absorption at 2.353 eV under high pump power, which could be attributed to the large amounts of carriers accumulated at the conduction band. Seldom previous researches have paid attention to this peak. Hot phonon bottleneck effect plays an important role in decelerating hot carrier cooling rate in this process. The high energy side of the photobleaching peak at 2.490 eV is found to have a close relationship with the carrier concentration and carrier cooling rate. It only appears in the first 100 fs after the

* Corresponding author.
E-mail address: chenr@sustech.edu.cn (R. Chen).
[c] These authors contributed equally to this work.

https://doi.org/10.1016/j.mtphys.2020.100228

arrival of the 442 nm fs pump pulse laser and then quickly disappears within 5 ps under high pump power. Under low pump power, however, no such bleaching peak can be found. While the high energy side photobleaching peak is decreasing, the ground state photobleaching peak at 1.634 eV and excited state absorption gradually increase until high energy side photobleaching peak disappears at 5 ps. An energy transfer is adopted to interpret the phenomenon observed herein. It is noted that large amounts of hot carriers induce significant Auger effect at not only the bandgap but also the higher conduction band, which keeps the carriers hot for more than 5 ns.

2. Materials and methods

2.1. Sample preparation

High-purity (99.99%) PbI_2 was purchased from Alfa Chemical Group, and methylammonium iodide (MAI) with a purity of more than 99.5% were purchased from Luminescence Technology Corp. To prepare $MAPbI_3$ solutions with a concentration of $1 mol/L$, MAI powders with the corresponding molar ratios, together with PbI_2, were added to dimethylformamide (DMF) and dimethyl sulfoxide (DMSO), which had a volume ratio of 7:3. Quantity of all these reagents is not hard to calculate. Then, all solutions were stirred at the rate of 300 rpm and heated at 60°C for 2 h. Before spin coating on quartz substrates, the solution was filtered with 0.22 μm polytetrafluoroethylene filters. Finally, thin films of about 250 nm were prepared, which had been estimated by transmission electron microscopy through the intramolecular exchange method. In addition, another quartz substrate was used to capsulate the thin film to avoid the degradation of sample. The films prepared by the above method are dense and uniform, which makes the structural and optical analyses of these samples meaningful.

2.2. Optical measurement

In the experiment, the 442 nm pump laser is generated in an ultrafast parametric amplifier (Coherent OperA Solo) by 800 nm fs laser of 1 kHz frequency and 93 fs pulse width from Astrella ultrafast Ti:sapphire laser device. The white laser which is used to measure the absorption of the sample is generated in CaF_2 crystal. The transient absorption spectra are measured by the ExciPro femtosecond pump-probe spectrometer (CDP Systems Corp.). An optical delay line is used to change the delay time between the pump and probe pulses. During the experiment, there are a little difference between the reflectance and transmittance of the quartz surface considering the human operating error and the power meter error. Therefore, we took the average reflectance 14.918% and average transmittance 2.875% for the relevant calculation process. In determining the pump power, the reflected pump light was subtracted to obtain more accurate carrier concentration calculation. The thickness of sample is about 250 nm, and the spot size of pump pulse and probe pulse are$7.85 \times 10^{-3} cm^2$and $1.77 \times 10^{-4} cm^2$, respectively.

3. Results and discussion

3.1. Carrier cooling

$MAPbI_3$ film spin-coated on a quartz substrate has been used to investigate the carrier dynamics in our experiment. The sample is pumped with 442 nm laser pulse of 92 fs and probed with a continuum white light generated by 800 nm laser pulse on CaF_2 crystal. Fig. 1 shows the transient absorption spectra of $MAPbI_3$ under low pump power (0.05 mW) and high pump power (1 mW), with carrier concentration corresponds to 4.66×10^{17} and 9.32×10^{18} cm^{-3}, respectively. The carrier concentration at the highest pump power is one order of magnitude higher than the previous research, which is 4×10^{17} cm^{-3} [17]. During our measurement, no damage of the sample has been observed, which demonstrates the good stability of our samples. The calculation of carrier concentration can be found in other research work [13]. There is only one ground state bleaching peak at 1.652 eV under the pump power of 0.05 mW, whereas two bleaching peaks at 1.646 and 2.516 eV can be found under the pump power of 1 mW. The dual peaks nature has been reported in many other works, but the origin is still under controversial discussion [25–27]. From Fig. 1(a) and (b), it can be seen that the ground state bleaching peak increases to a maximum at around 3 ps and then declines to almost zero at around 5 ns. In comparison, transient absorption spectra under the pump power of 1 mW exhibits different trends as shown in Fig. 1(c) and (d). In the first 100 fs, there is one photobleaching peak at 2.516 eV accompanied with positive signal at all other energy positions. This is because of the strong electron scattering at the energy position of 2.516 eV induced by the high concentration of electrons.

To explain clearly, a possible schematic energy band structure is adopted here as shown in Fig. 2(a) [28,29]. Electron transition between two valence bands and lower conduction band proposed in other work are inappropriate here [26]. As depicted in Fig. 2(a), solid yellow circles are electrons in the conduction band, whereas open white circles are holes in the valence band. Two conduction bands are denoted as conduction band 1 and conduction band 2. The transition of electrons from valence band to the conduction band 1 is indicated by black arrows and the transition of electrons from the conduction band 1 to the conduction band 2 is shown as red arrows. These two transitions are ascribed to ground state bleaching and excited states absorption, respectively. The electron scattering originated from the energy position of 2.516 eV is too fast to resolve in the experiment because the scattering time is less than 100 fs as seen in Fig. 1(c), whereas the laser pulse duration is 92 fs. This electron scattering process could also be named as carrier thermalization, during which electrons will be scattered into a Maxwell-Boltzmann distribution and then cool to the bottom of the conduction band 1. As the delay time increases to more than 100 fs, the photobleaching peak at 2.516 eV decreases. At the same time, ground state bleaching peak at 1.646 eV and excited state absorption at 2.353 eV start to increase. This excited state absorption has not drawn enough attention before because it only appears under much higher pump power. There are only a few papers that observed similar signal; however, no detail analysis has been carried out [30]. Peaks at the energy position around 1.5 eV come from the 800 nm laser pulse and will not be considered herein. Fig. 1(a) and (c) plot the carrier cooling process under low and high pump power, respectively. The reason why the photobleaching peak exists on the high energy side under high pump power (while it is absent for low pump power) is that the electron concentration is too high in the first situation to inhibit the electron cooling. Carriers could stay at the energy position of 2.516 eV for a long time and subsequently, induce a bleaching peak. The carrier recombination appears after the carrier cooling, and it still shows huge difference under low and high pump power. The ground state bleaching peak under the pump power of 0.05 mW declines to almost zero within 5 ns. In the case of 1 mW, not only the ground state bleaching peak but also the excited state absorption peak persist a considerable value when the delay time is 5 ns. The trend would last for a much longer time which exceeds the delay range in our experiment. The detail carrier recombination process will be discussed in the following section. Transient absorption spectra under different pump powers are shown in Fig. S1. With the increase of pump

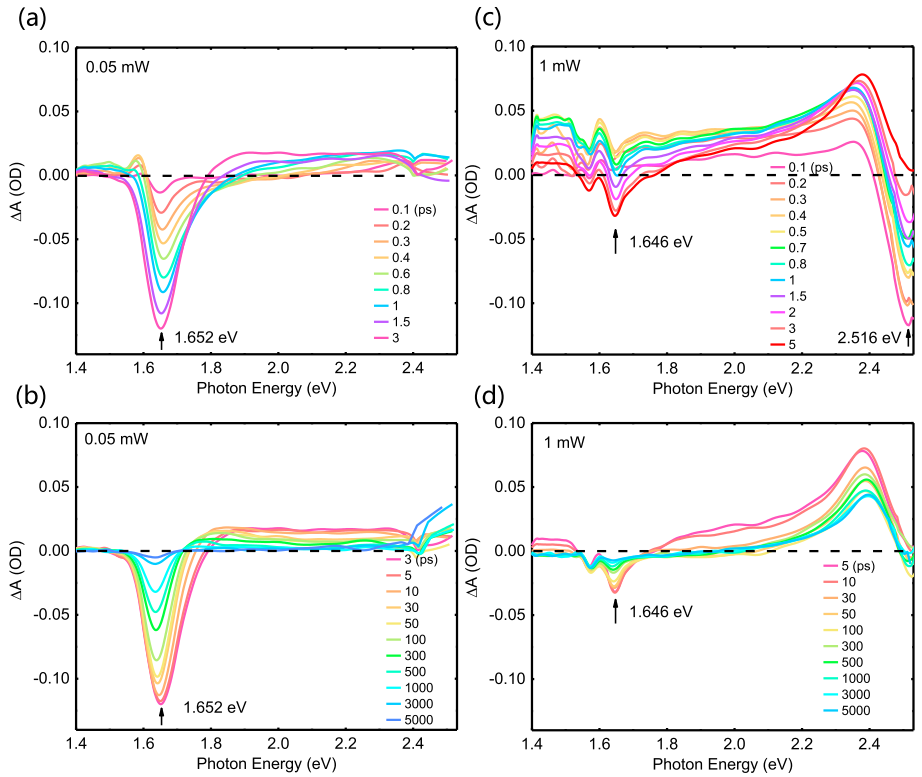

Fig. 1. Transient absorption spectra of $MAPbI_3$ under pump power of 0.05 mW and 1 mW, correspond to carrier concentration of 4.66×10^{17} cm^{-3} and 9.32×10^{18} cm^{-3}, respectively. (a) Pump power: 0.05 mW, delay time range: 0–3 ps. (b) Pump power: 0.05 mW, delay time range: 3–5000 ps. (c) Pump power: 1 mW, delay time range: 0–5 ps. (d) Pump power: 1 mW, delay time range: 5–5000 ps.

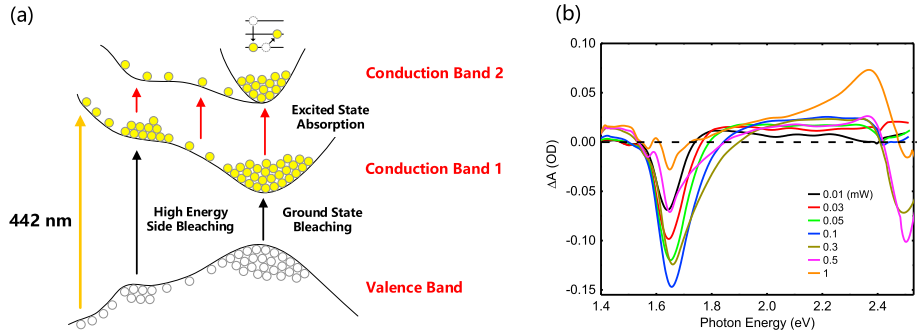

Fig. 2. (a) Schematic of the energy band structure and electron transition of $MAPbI_3$ under the excitation of 442 nm laser pulse with a duration of 92 fs. (b) Transient absorption spectra of $MAPbI_3$ under different excitation power at the time the carrier cooling completes.

power, the ground state bleaching peaks become wider, and the photobleaching peaks gradually appear around 2.516 eV. The increase of the peak width can be attributed to the Burstein-Moss shift [16]. On the other hand, excited state absorption peaks exist with intensity increasing simultaneously. Fig. S2 shows the normalized decay curves in the first 10 ps of $MAPbI_3$ at 1.652 eV under different pump powers. It can be seen clearly that the signal increase to the maximum when the delay time is around 3 ps. For the situation of high pump power, the decay time is about 5 ps, which is a little bit longer than the others. This implies that the carrier cooling time is between 3 and 5 ps in the material and after this time scale, carriers start to recombine. During the carrier cooling process, the ground state bleaching peak position varies with the delay time. The peak shifting can be ascribed to the Burstein-Moss effect and bandgap renormalization, which results in a blue-shift and red-shift, respectively [31–33].

Fig. 2(b) shows the transient absorption spectra of $MAPbI_3$ under different pump powers when the ground state bleaching signal reaches the maximum, at which the carrier cooling process finished. It can be seen obviously that only ground state bleaching peaks appear under low pump power (0.01, 0.03, 0.05 and 0.1 mW). When the pump power exceeds 0.1 mW, another photobleaching peak appears around 2.5 eV because of the strong carrier scattering induced by the high concentration of carriers at this energy position. The excited state absorption around 2.353 eV starts to dominate the transient absorption. Meanwhile, the amplitude of the photobleaching peak located at the low energy side decreases significantly.

It has been discussed that there is an energy transfer under high pump power. To show this process clearly, normalized decay curves at the photon energy 1.634, 2.353, and 2.490 eV under different pump powers have been plotted in Fig. 3. Energy transfer happens

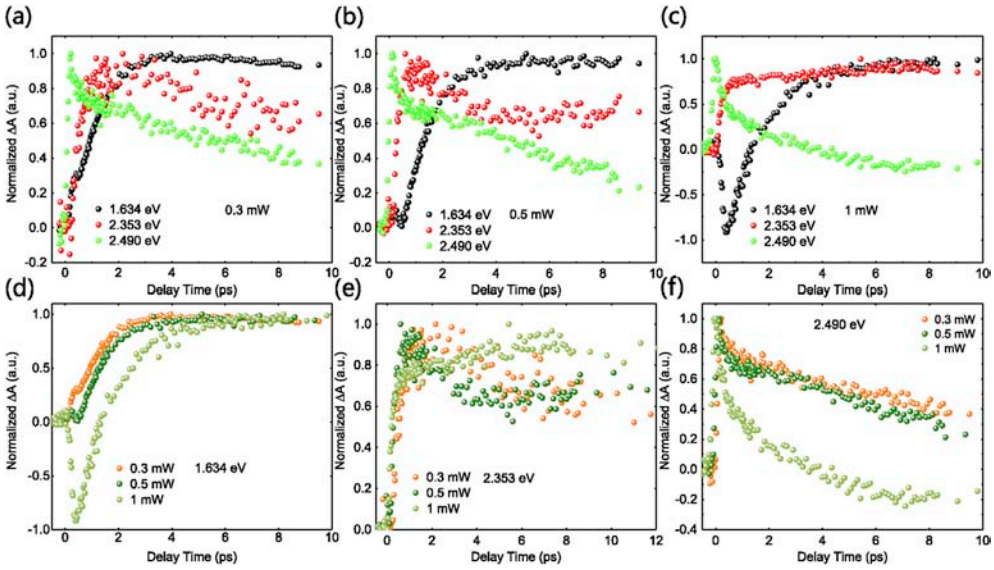

Fig. 3. (a)–(c) Normalized decay curves in the range of 0–10 ps at photon energy of 1.634, 2.353, and 2.490 eV under the pump power of 0.3, 0.5 and 1 mW, respectively. (d)–(f) Normalized decay curves in the range of 0–10 ps under pump power of 0.3, 0.5, and 1 mW at photon energy of 1.634, 2.353, and 2.490 eV, respectively.

in the carrier cooling process, and therefore, the early 10 ps period is selected for comparison here. As shown in Fig. 3(a), it can be seen that after the arrival of the pump laser pulse, the amplitude of high energy side bleaching increases most quickly and begin to decrease at the delay time of 200 fs. At the same time, the ground state bleaching and the excited state absorption peaks increase. Obviously, the energy transfer, that is, the electrons cooling happens from the high energy position to the bottom of the conduction band 1. The situation under the pump power of 0.5 mW is similar to that of 0.3 mW. Carrier cooling time is a little longer when the pump power is higher because the low energy side photobleaching peak increases for a longer time under the pump power of 0.5 mW. Hot phonon bottle effect is considered to contribute to this phenomenon. Decay curves under the pump power of 1 mW show significant differences. As shown in Fig. 3(c), the excited state absorption peak shows an increase at first and then decreases with time. The early process is very fast and only lasts for 500 fs. Then, it decreases slowly until almost 10 ps. Ground state bleaching peak is different from that under lower pump power. The amplitude of the peak decreases to negative values firstly and then increases. Here, it is needed to emphasize that we have normalized the minus value of the ground state bleaching signal in Fig. 3(c) for easier comparison. It is interesting to find that the decrease time of the ground state bleaching is the same as that of the fast increase of the excited state absorption peak. This implies that the two processes must derivate from the same mechanism. As shown in Fig. 1(c), the strong carrier scattering will lead to a rapidly rising of wide-band excited state absorption after optical pumping, as indicated by the red arrows in Fig. 2(a). During this period, the blocking of carrier transition from valence band to conduction band 1 will generate the negative ground state bleaching signal, as indicated by the black arrow in Fig. 2(a). The excited carriers gradually relax to the bottom of conduction band 1, which leads to the narrowing of the excited state absorption signal. Owing to the overlapping of the strong and wide positive excited state absorption, the negative ground state bleaching signal is lifted. This is why the ground state bleaching signal remains positive at the very beginning, as shown in Fig. 1(c). For longer time region as shown in Fig. 1(d), the influence of excited state absorption can be ignored because of its narrowing. Then, the ground state bleaching signal will maintain at negative value. As discussed above, the physical mechanism of this phenomenon should be attributed to the carrier scattering induced by the high concentration of electrons at the energy position of 2.490 eV. Actually, this process is the carrier thermalization which has been mentioned in other work [17]. Fig. 3(d) and (f) show three decay curves under different pump powers. The carrier dynamics is almost the same under the pump power of 0.3 and 0.5 mW, which can be identified by the overlapping of two curves. Decay curves under the pump power of 1 mW are different because the carrier scattering plays an important role in the first 500 fs induced by the high concentration of electrons.

To characterize the carrier cooling, the carrier temperature T_c is extracted by fitting the high energy tail of the transient absorption spectra above the band edge [34–36]. When pumped by the femtosecond pulse laser, carriers inside the sample satisfy a Maxwell-Boltzmann distribution characterized by Equation (1) [10], where ΔA is the transient absorption amplitude, C is constant, $h\nu$ is the photon energy, and k_b is the Boltzmann constant. The red lines in Fig. 4(a) are the fitting results of the transient absorption spectra under pump power of 0.1 mW.

$$\Delta A = Ce^{-h\nu/k_bT_c} \tag{1}$$

The carrier temperature T_c under other pump powers have also be extracted as shown in Fig. 4(b). Carrier temperature under pump power of 0.5 and 1 mW is not shown here because the excited state absorption signal is so strong that the high energy tail is not a Maxwell-Boltzmann distribution as shown in Fig. 1(c) and (d). From Fig. 4(b), it can be seen that the initial carrier temperature become higher with the increase of pump power. This implies that carriers take longer time to cool down from initial temperature to ambient temperature under high pump power. Hot phonon bottle effect should be responsible for this phenomenon. Besides, the cooling process could be divided into two stages, as reported before [9]. The first stage is dominated by the interaction between electron and longitudinal optical phonon [37], whereas the second corresponds to a hot phonon bottleneck effect. Previous researches usually focus on the band filling at the band gap caused by either carrier cooling or ground state bleaching [9,13,38]. It has been intensively investigated that the Burstein-Moss shift is related to the band gap

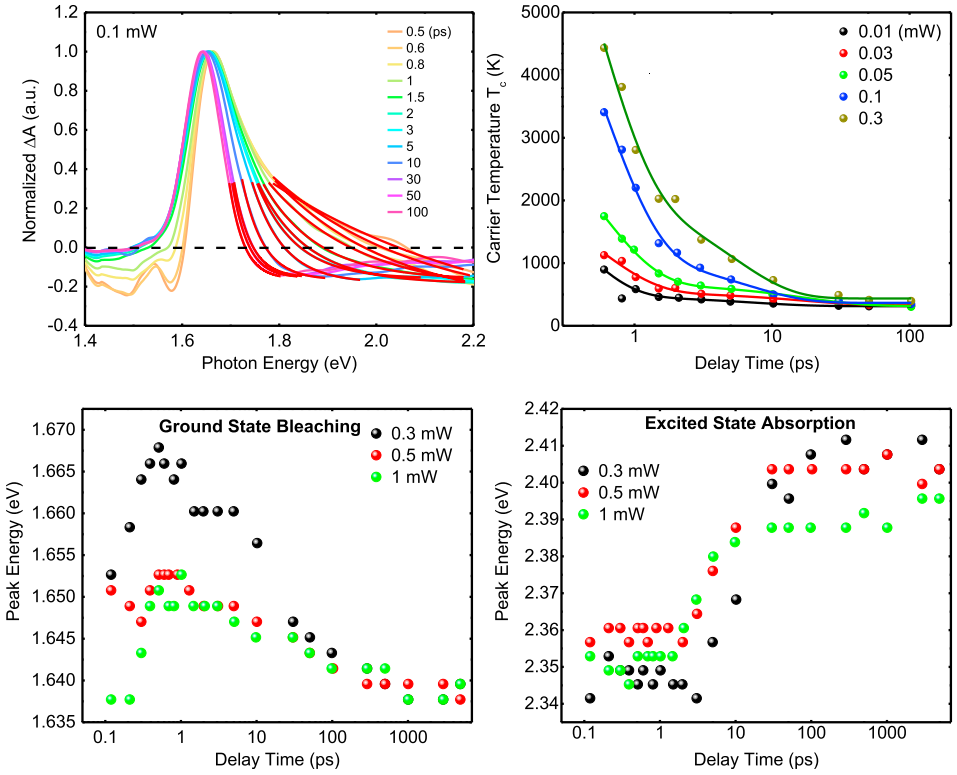

Fig. 4. (a) Fitting of transient absorption spectra tails of $MAbI_3$ under the pump power of 0.1 mW to extract carrier temperature T_c at different delay times. (b) Fitting curves of carrier temperature T_c under different pump powers. (c) Peak position of the low energy side photobleaching peak under high pump power of 0.3, 0.5, and 1 mW as delay time increases. (d) Peak position of the excited state absorption under high pump power of 0.3, 0.5, and 1 mW as delay time increases.

because of the band filling. In this work, it has been found that the carrier cooling induced the band filling effect influences not only the ground state bleaching but also the excited state absorption, as shown in Fig. 4(c) and (d), which plot the peak evolution of the ground state bleaching and excited state absorption, respectively. The ground state bleaching peak firstly moves to the high energy side within around 1 ps. This implies the carrier cooling and then the cooled electrons accumulate at the bottom of the conduction band 1. Excess electrons cooled from the high energy band later have to occupy higher energy state at the bottom of the lower conduction band because of the Pauli Exclusion Principle. After around 1 ps, the ground state bleaching peak starts to shift to lower energy side, and this could be attributed to carrier recombination or band depletion. Carriers accumulate not only at the bottom of the conduction band 1 but also the bottom of conduction band 2, as shown in Fig. 2(a). In the first 5 ps, the peak position nearly keeps identical. This corresponds to the carrier cooling to the bottom of the conduction band 1. The amplitude of excited state absorption is proportional to the concentration of electrons at the bottom of the conduction band 1. The more electrons at the bottom of the conduction band 1, the more electrons at the bottom of the conduction band 2. Around 5 ps later, the peak of the excited state absorption shifts to higher energy side. This phenomenon should be caused by carrier recombination, which takes more energy for electrons to transit from the conduction band 1 to the conduction band 2. This trend corresponds to the peak shift of the ground state bleaching very well. The band filling and band depletion discussed here only appear under the high pump power, and therefore, the high concentration of carriers accumulated in the bottom of conduction band 1 should be an important factor. A significant Auger effect happens here, which slows down the carrier transition between two conduction bands and the recombination between the conduction band 1 and valence band.

3.2. Carrier recombination

Auger effect is a result of the high concentration of carriers under high pump power. It has a significant influence on the carrier recombination and therefore is crucial for carrier extraction in hot carrier device. To investigate the recombination mechanism inside the $MAPbI_3$ under different pump powers, several recombination theories have been adopted to fit the decay curves, as shown in Fig. 5. Fig. 5(a) shows the decay curves at the bandgap under pump power of 0.01–0.3 mW, which is regarded as lower pump power regime. Decay curves under the pump power of 0.5 and 1 mW, which are regarded as high pump power here, are shown in Fig. 4(b). Recombination kinetics under different pump powers is different. Equation (2) indicates the recombination dynamics is closely related to carrier concentration. Here n is the carrier concentration, and A, B, and C are coefficients of the first order, the second order, and the third order recombination, respectively. For $MAPbI_3$, free electrons and holes are the main carriers at room temperature. Therefore, the first order is mainly the defects mediated recombination, whereas the second order is free electron-hole recombination, and the third order is Auger recombination.

$$-\frac{dn}{dt} = An + Bn^2 + Cn^3 \tag{2}$$

Under lower pump power, as shown in Fig. 5(a), recombination regimes after 2000 ps is almost the same as the decay curves overlap with each other. The carrier concentration at this time is

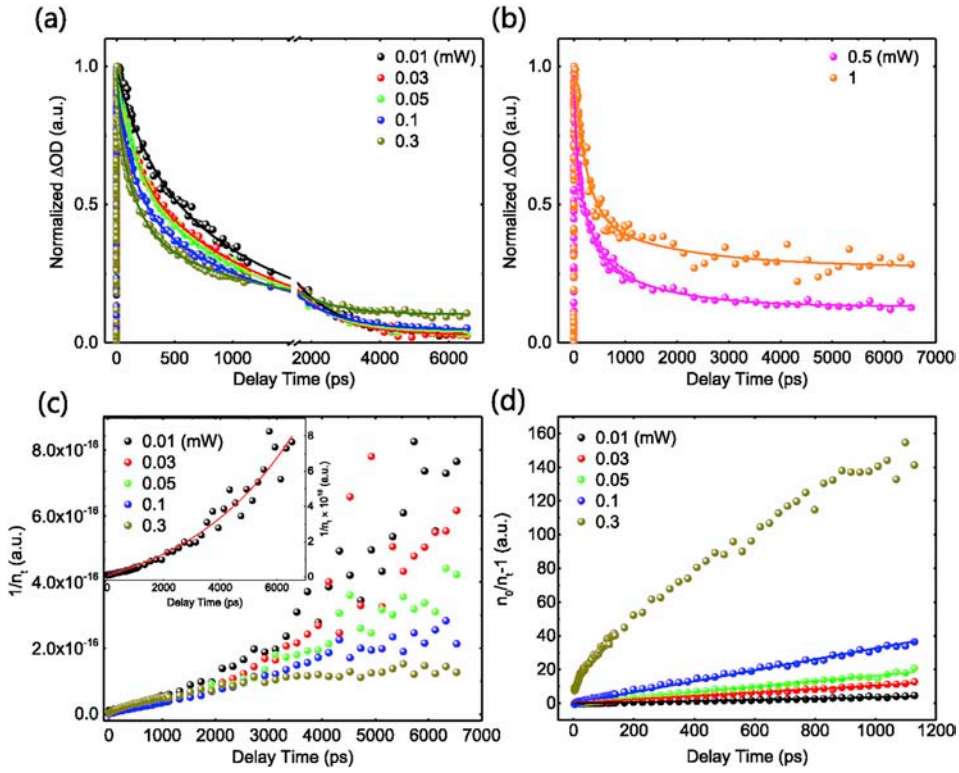

Fig. 5. (a) Normalized decay curves and the corresponding fitting curves of $MAPbI_3$ under different excitation powers. (b) Normalized decay curve and corresponding fitting curves of $MAPbI_3$ under the high excitation power of 0.5 and 1 mW. (c) $1/n_t$, where n_t is the carrier concentration, as a function of delay time under different excitation powers. Inset is the fitting curve under the excitation power of 0.01 mW. (d) $(1/n_t - 1)$ as a function of delay time under different excitation powers and corresponding fitting curves. For 0.3 mW, the curve deviates from other situations and is not fitted.

very low, and the recombination here is mainly mediated by defects. Before the delay time of 2000 ps, the recombination kinetics is obviously different. The recombination rate increases with the increase of the pump power. To make sure that the first two components work in the recombination process, the coefficient C in Equation (2) is set to be zero, that is, only the defects-mediated recombination and free electron-hole recombination are considered. And then, Equation (2) can be rewritten as Equation (3).

$$-\frac{dn}{dt} = An + Bn^2 \tag{3}$$

Integrate Equation (3), we can get

$$\frac{1}{n_t} = \left(\frac{1}{n_0} + \frac{B}{A}\right)e^{At} - \frac{B}{A} \tag{4}$$

Here n_t is the carrier concentration related to the ground state bleaching at the delay time t, and n_0 is the carrier concentration at the initial time. Fig. 5(c) shows $1/n_t$ as a function of delay time. It can be seen that the variation of $1/n_t$ under the pump power of 0.3 mW is different from that under the lower pump power. The inset of Fig. 5(c) shows the well-fitting of the data for the case of 0.01 mW, which indicating that the carrier recombination dynamics consists of two components discussed above. Situations about 0.03, 0.05, and 0.1 mW are similar to that of 0.01 mW, and the fitting curves are shown in Fig. S3. The fitting result is listed in Table 1, where it can be seen that the average defects-mediated recombination rate A is around 1.879×10^8 s^{-1}, and the second order recombination coefficient B is around 3.785×10^{-8} cm^3s^{-1}. Although there are some differences of these values for different pump powers, the magnitude is the same, and it is the inner property of $MAPbI_3$. The unit of n_0B is s^{-1}, represents the second order recombination rate and is of the magnitude of 10^{10} s^{-1}.

Table 1
Fitting results of the whole delay time range using Equation (4).

Pump Power (mW)	0.01	0.03	0.05	0.10
n_0 (cm^{-3})	9.32×10^{16}	2.79×10^{17}	4.66×10^{17}	9.32×10^{17}
A (s^{-1})	2.52×10^8	2.46×10^8	1.54×10^8	1.02×10^8
B (cm^3s^{-1})	4.50×10^{-8}	3.69×10^{-8}	3.87×10^{-8}	3.08×10^{-8}
n_0B (s^{-1})	4.19×10^9	1.03×10^{10}	1.80×10^{10}	2.87×10^{10}

To investigate the recombination regime of the first period, the first 1200 ps of the whole process has been extracted as shown in Fig. 5(d). During this period, the $(n_0/n_t\text{-}1)$~ t curves from 0.01 to 0.1 mW display a linear trend corresponding to the second order recombination [14]. To clarify this point, only the second order recombination rate in Equation (2) is considered for this period. So, the Equation (2) can be rewritten as Equation (5).

$$-\frac{dn}{dt} = Bn^2 \tag{5}$$

Integrate Equation (5), we can get

$$\frac{n_0}{n_1} - 1 = n_0Bt \tag{6}$$

Therefore, $(n_0/n_t\text{-}1)$ is linearly dependent on the delay time t, and n_0B is the slope of these curves. By fitting the data based on Equation (6), the average value of the second order recombination coefficient B is determined to be 3.65×10^{-8} cm^3s^{-1} for different pump powers, which is in the same magnitude of that in Table 1, implying the analysis above is reasonable. It is needed to mention

that the coefficients determined above are meaningful. The specific fitting values can be found in Table 2. The value of n_0B determined here is also of the 10^{10} s^{-1} magnitude, which is the same as that in the global range fitting for $MAPbI_3$. When the pump power becomes higher, the second order recombination rate is larger. The term $(n_0/n_t\text{-}1)$ under pump power of 0.3 mW deviates from the linear trend because the carrier concentration is too high, and there must be additional recombination regimes such as Auger recombination. To prove this point, decay curves under different pump powers have been fitted by exponential functions as shown in Fig. 5(a) and (b) using Equation (7). Fitting results are shown in Table 3.

$$y = A_1 e^{-x/t_1} + A_2 e^{-x/t_2} + A_3 e^{-x/t_3} \quad (7)$$

From Table 3, it can be seen that for low pump power from 0.01 to 0.05 mW, only two exponential terms fit the decay curves well, whereas under the pump power of 0.1 and 0.3 mW, three exponential terms are needed. Pump power of 0.1 mW is a critical value where three exponential terms are able to fit the decay curve well instead of two. This means that under low pump power, there is no Auger recombination until the pump power increase up to 0.1 mW with a carrier concentration of 9.32×10^{17} cm^{-3}. The time constants t_3 for different pump powers is the same with a value of around 1200 ps. It corresponds to the Fig. 5(a) very well because the tails of decay curves overlap with each other except that of 0.3 mW, and t_3 is actually the time constants for defect-mediated recombination. Besides, the start point of the tails is almost the same which indicates that the recombination activity is carrier-concentration dependent. Carriers recombine in a specific manner at the specific concentration. What is more, the time constants t_2 which corresponds to the free electron-hole recombination for pump power from 0.03 to 0.3 mW are about 160 ps. The time constants t_2 for the situation of 0.01 mW is longer with a value of 263.50 ps because the recombination rate is too slowly. Nevertheless, these time constants are of the same magnitude and reasonable. With the further increase of pump power up to 0.1 mW, the Auger recombination appears, and the time constant t_1 for this period is 10.63 ps. The time constant t_1 becomes longer when the pump power increases to 0.3 mW.

Auger recombination is stronger when the pump power is higher as shown in Fig. 5(b). The specific time constants cannot be decided because the curve tail possesses a large value. More time beyond the time range in the experiment is needed to wait for the transient absorption signal decrease to zero. When the pump power is high enough such as 1 mW as shown in Fig. 5(b), carriers keep hot for more than 6 ns obviously. A high concentration of carriers under this condition accumulates at the bottom of the conduction band, and the recombination is slowed down because of the Auger effect. A lot of carriers on the high energy level can be rapidly extracted, and therefore, the PCE can be further improved under high pump power. This is crucial for hot carrier devices. Both hot phonon bottleneck effect and Auger recombination are meaningful for the hot carrier electronics. And the pump power is crucial to generate lots of hot carriers. In $MAPbI_3$, the existence of the two effects derived from its unique structure. The two-conduction-band structure provides more energy states for electrons to accumulate.

Table 2
Fitting results of the second order recombination using Equation (6).

Pump Power (mW)	0.01	0.03	0.05	0.1
n_0 (cm^{-3})	9.32×10^{16}	2.79×10^{17}	4.66×10^{17}	9.32×10^{17}
B (cm^3s^{-1})	3.94×10^{-8}	3.68×10^{-8}	3.50×10^{-8}	3.50×10^{-8}
n_0B (s^{-1})	3.67×10^{9}	1.03×10^{10}	1.63×10^{10}	3.26×10^{10}

Table 3
Fitting results of the ground state bleaching decay curves using Equation (7).

Pump Power (mW)	A_1	t_1 (ps)	A_2	t_2 (ps)	A_3	t_3 (ps)
0.01	–	–	0.29	263.50	0.67	1266.29
0.03	–	–	0.31	152.30	0.61	1206.34
0.05	–	–	0.36	160.51	0.57	1159.01
0.10	0.12	10.63	0.41	158.16	0.46	1247.96
0.30	0.24	17.52	0.39	163.04	0.32	1174.45

Under high pump power, high concentration of electrons will be generated and subsequently induce significant Auger effect at two conduction bands. For the conduction band 2, that is, the excited state absorption, Auger effect mainly inhibits the intraband relaxation. Therefore, a lot of hot carriers accumulate at the high energy level and the excited state absorption persist a considerable value. The Auger effect also happens at the bottom of conduction band 1 and then slow down the recombination between electrons and holes at valence band. This is also meaningful for the hot carriers extraction as long as the extraction time is less than the carrier lifetime.

4. Conclusion

$MAPbI_3$ exhibits unique transient absorption properties under high pump power. The energy structure with two conduction bands is proposed here. The appearance of the high energy side bleaching peak at 2.353 eV can be attribute to the energy transfer from high energy level to the bottom of the conduction band 1, and a strong carrier-band filling effect happens during the energy transfer time. The unique and significant excited state absorption is observed under high pump power, which is ascribed to the high concentration of carriers at the conduction band 1. This is a strong evidence for the two-conduction band structure of $MAPbI_3$. Carriers keep hot, that is, stay at the high energy level for more than 5 ns, and this could be explained by Auger effect. Surprisingly, Auger effect exists not only at the conduction band 1 but also the conduction band 2. Subsequently, the excited state absorption and the ground state bleaching signals persist for more than 5 ns. A critical carrier concentration of 9.32×10^{17} cm^{-3} is determined for this effect to happen. The result is meaningful for further understanding of carrier dynamics of perovskite materials and its application in optoelectronic devices.

Credit author statement

G.T.P., B.A.C., and R.C. conceived the experiment. X.Q.L. and Z.B.H. was responsible for the preparation of $MAPbI_3$ films, including the film encapsulation. B.A.C. and G.T.P. carried out the ultrafast transient absorption experiments and worked on the data analysis. All authors discussed the data and contributed to the manuscript.

Data availability

The raw/processed data required to reproduce these findings cannot be shared at this time due to technical or time limitations.

Declaration of competing interest

The authors declare that they have no known competing financial interests or personal relationships that could have appeared to influence the work reported in this paper.

Acknowledgments

This work is supported by the National Natural Science Foundation of China (11574130), Shenzhen Science and Technology Innovation Commission (Projects Nos. KQJSCX20170726145748464, JCYJ20180305180553701, and KQTD2015071710313656).

Appendix A. Supplementary data

Supplementary data to this article can be found online at https://doi.org/10.1016/j.ijhydene.2020.05.057.

References

[1] C. Wehrenfennig, G.E. Eperon, M.B. Johnston, H.J. Snaith, L.M. Herz, High charge carrier mobilities and lifetimes in organolead trihalide perovskites, Adv. Mater. 26 (2014) 1584–1589, https://doi.org/10.1002/adma.201305172.
[2] T.J. Savenije, et al., Thermally activated exciton dissociation and recombination control the carrier dynamics in organometal halide perovskite, J. Phys. Chem. Lett. 5 (2014) 2189–2194, https://doi.org/10.1021/jz500858a.
[3] S. D Stranks, et al., Electron-hole diffusion lengths exceeding 1 micrometer in an organometal trihalide perovskite absorber, Science 342 (2013) 341–344, https://doi.org/10.1126/science.1243982.
[4] C.S. Ponseca, et al., Organometal halide perovskite solar cell materials rationalized: ultrafast charge generation, high and microsecond-long balanced mobilities, and slow recombination, J. Am. Chem. Soc. 136 (2014) 5189–5192, https://doi.org/10.1021/ja412583t.
[5] S.N. Vijayaraghavan, J. Wall, L. Li, G. Xing, Q. Zhang, F. Yan, Low-temperature processed highly efficient hole transport layer free carbon-based planar perovskite solar cells with SnO_2 quantum dot electron transport layer, Mater. Today. Phys. 13 (2020) 100204, https://doi.org/10.1016/j.mtphys.2020.100204.
[6] A decade of perovskite photovoltaics, Nat. Energy. 4 (2019), https://doi.org/10.1038/s41560-018-0323-9, 1-1.
[7] Z. Chen, et al., Single-crystal $MAPbI_3$ perovskite solar cells exceeding 21% power conversion efficiency, ACS Energy Lett 4 (2019) 1258–1259, https://doi.org/10.1021/acsenergylett.9b00847.
[8] W.S. Yang, et al., Iodide management in formamidinium-lead-halide–based perovskite layers for efficient solar cells, Science 356 (2017) 1376–1379, https://doi.org/10.1126/science.aan2301.
[9] J. Yang, et al., Acoustic-optical phonon up-conversion and hot-phonon bottleneck in lead-halide perovskites, Nat. Commun. 8 (2017) 14120, https://doi.org/10.1038/ncomms14120.
[10] M. Li, et al., Slow cooling and highly efficient extraction of hot carriers in colloidal perovskite nanocrystals, Nat. Commun. 8 (2017) 14350, https://doi.org/10.1038/ncomms15299.
[11] M.B. Price, et al., Hot-carrier cooling and photoinduced refractive index changes in organic-inorganic lead halide perovskites, Nat. Commun. 6 (2015) 8420, https://doi.org/10.1038/ncomms9420.
[12] P. Papagiorgis, L. Protesescu, M.V. Kovalenko, A. Othonos, G. Itskos, Long-lived hot carriers in formamidinium lead iodide nanocrystals, J. Phys. Chem. C 121 (2017) 12434–12440, https://doi.org/10.1021/acs.jpcc.7b02308.
[13] Y. Yang, et al., Observation of a hot-phonon bottleneck in lead-iodide perovskites, Nat. Photon. 10 (2015) 53–59, https://doi.org/10.1038/NPHOTON.2015.213.
[14] Y. Wu, et al., New group V graphyne: two-dimensional direct semiconductors with remarkable carrier mobilities, thermoelectric performance, and thermal stability, Mater. Today. Phys. 12 (2020) 100164, https://doi.org/10.1016/j.mtphys.2019.100164.
[15] W. Shockley, H.J. Queisser, Detailed balance limit of efficiency of p-n junction solar cells, J. Appl. Phys. 32 (1961) 510, https://doi.org/10.1063/1.1736034.
[16] J.S. Manser, P.V. Kamat, Band filling with free charge carriers in organometal halide perovskites, Nat. Photon. 8 (2014) 737–743, https://doi.org/10.1038/NPHOTON.2014.171.
[17] J.M. Richter, et al., Ultrafast carrier thermalization in lead iodide perovskite probed with two-dimensional electronic spectroscopy, Nat. Commun. 8 (2017) 376, https://doi.org/10.1038/s41467-017-00546-z.
[18] A. Mondal, et al., Ultrafast exciton many-body interactions and hot-phonon bottleneck in colloidal cesium lead halide perovskite nanocrystals, Phys. Rev. B 98 (2018) 115418, https://doi.org/10.1103/PhysRevB.98.115418.
[19] L.M. Herz, Charge-carrier dynamics in organic-inorganic metal halide perovskites, Annu. Rev. Phys. Chem. 67 (2016) 65–89, https://doi.org/10.1146/annurev-physchem-040215-112222.
[20] N. Ueda, H. Maeda, H. Hosono, H. Kawazoe, Band-gap widening of CdO thin films, J. Appl. Phys. 84 (1998) 6174–6177, https://doi.org/10.1063/1.368933.
[21] D. Huang, J.I. Chyi, H. Morkoç, Carrier effects on the excitonic absorption in GaAs quantum-well structures: phase-space filling, Phys. Rev. B 42 (1990) 5147–5153, https://doi.org/10.1103/PhysRevB.42.5147.
[22] J.M. Wiesenfeld, A.J. Taylor, Picosecond band filling in highly excited In-Ga-As-P films, Phys. Rev. B 34 (1986) 8740–8749, https://doi.org/10.1103/PhysRevB.34.8740.
[23] B. Hejda, K. Kral, Hot-electron cooling and second-generation phonons in polar semiconductors, Phys. Rev. B 47 (1993) 15554–15561, https://doi.org/10.1103/PhysRevB.47.15554.
[24] R.P. Joshi, D.K. Ferry, Hot-phonon effects and interband relaxation processes in photoexcited GaAs quantum wells, Phys. Rev. B 39 (1989) 1180–1187, https://doi.org/10.1103/PhysRevB.39.1180.
[25] K.G. Stamplecoskie, J.S. Manser, P.V. Kamat, Dual nature of the excited state in organic–inorganic lead halide perovskites, Energy Environ. Sci. 8 (2015) 208–215, https://doi.org/10.1039/c4ee02988g.
[26] G. Xing, et al., Long-range balanced electron-and hole-transport lengths in organic-inorganic $CH_3NH_3PbI_3$, Science 342 (2013) 344–347, https://doi.org/10.1126/science.1243167.
[27] I. Minda, J. Horn, E. Ahmed, D. Schlettwein, H. Schwoerer, Ultrafast charge dynamics in mixed cation-mixed halide perovskite thin films, ChemPhysChem 19 (2018) 3010–3017, https://doi.org/10.1002/cphc.201800547.
[28] J. Even, et al., Solid-state physics perspective on hybrid perovskite semiconductors, J. Phys. Chem. C 119 (2015) 10161–10177, https://doi.org/10.1021/acs.jpcc.5b00695.
[29] J. Even, L. Pedesseau, C. Katan, Analysis of multivalley and multibandgap absorption and enhancement of free carriers related to exciton screening in hybrid perovskites, J. Phys. Chem. C 118 (2014) 11566–11572, https://doi.org/10.1021/jp503337a.
[30] P. Piatkowski, B. Cohen, S. Kazim, S. Ahmad, A. Douhal, How photon pump fluence changes the charge carrier relaxation mechanism in an organic-inorganic hybrid lead triiodide perovskite, Phys. Chem. Chem. Phys. 18 (2016) 27090–27101, https://doi.org/10.1039/c6cp02682f.
[31] M. Feneberg, et al., Band gap renormalization and Burstein-Moss effect in silicon- and germanium-doped wurtzite GaN up to 10^{20} cm^{-3}, Phys. Rev. B 90 (2014): 075203, https://doi.org/10.1103/PhysRevB.90.075203.
[32] K.G. Saw, N.M. Aznan, F.K. Yam, S.S. Ng, S.Y. Pung, New insights on the Burstein-Moss shift and band gap narrowing in indium-doped zinc oxide thin films, PloS One 10 (2015): e0141180, https://doi.org/10.1371/journal.pone.0141180.
[33] M. Muñoz, F.H. Pollak, M. Kahn, D. Ritter, L. Kronik, G.M. Cohen, Burstein-Moss shift of n-doped $In_{0.53}Ga_{0.47}As$/InP, Phys. Rev. B 63 (2001) 233302, https://doi.org/10.1103/PhysRevB.63.233302.
[34] J.F. Ryan, et al., Time-resolved photoluminescence of two-dimensional hot carriers in GaAs-AlGaAs heterostructures, Phys. Rev. Lett. 53 (1984) 1841–1844, https://doi.org/10.1103/PhysRevLett.53.1841.
[35] D. von der Linde, R. Lambrich, Direct measurement of hot-electron relaxation by picosecond spectroscopy, Phys. Rev. Lett. 42 (1979) 1090–1093, https://doi.org/10.1103/PhysRevLett.42.1090.
[36] D. Zanato, N. Balkan, B.K. Ridley, G. Hill, W.J. Schaff, Hot electron cooling rates via the emission of LO-phonons in InN, Semicond. Sci. Technol. 19 (2004) 1024–1028, https://doi.org/10.1088/0268-1242/19/8/013.
[37] H. Kawai, G. Giorgi, A. Marini, K. Yamashita, The mechanism of slow hot-hole cooling in lead-iodide perovskite: first-principles calculation on carrier lifetime from electron-phonon interaction, Nano Lett. 15 (2015) 3103–3108, https://doi.org/10.1021/acs.nanolett.5b00109.
[38] J. Fu, et al., Hot carrier cooling mechanisms in halide perovskites, Nat. Commun. 8 (2017) 1300, https://doi.org/10.1038/s41467-017-02301-w.